Bremsstrahlung of 5–25-keV electron impact with Al, Cu, Ag, Te, and Au thick solid targets with no polarization contribution

Ling Li (李玲), Zhu An (安竹),* Jingjun Zhu (朱敬军),† Wenjing Tan (谭文静), Qi Sun (孙琦), and Mantian Liu (刘慢天)
Key Laboratory of Radiation Physics and Technology of Ministry of Education, Institute of Nuclear Science and Technology, Sichuan University, Chengdu 610064, People's Republic of China

(Received 17 August 2018; revised manuscript received 2 January 2019; published 6 May 2019)

Bremsstrahlung spectra generated by electrons with incident energies of 5–25 keV bombarding thick targets of Al ($Z = 13$), Cu ($Z = 29$), Ag ($Z = 47$), Te ($Z = 52$), and Au ($Z = 79$) are measured with high accuracy. Comparing the experimental spectra with the simulated spectra obtained from the Monte Carlo code PENELOPE, it is found that they are in excellent agreement. The PENELOPE code contains only the cross sections for ordinary bremsstrahlung, while disregarding polarization bremsstrahlung. The results quite definitely indicate that there is no polarization bremsstrahlung contribution to the x-ray radiation spectra produced by incident electrons with thick solid targets for the x-ray energies of interest in this paper (>1 keV).

DOI: 10.1103/PhysRevA.99.052701

I. INTRODUCTION

There are two mechanisms of bremsstrahlung produced by electron impact (EB). One is ordinary bremsstrahlung (OB), which means continuous photon spectra generated by incident electrons accelerated in the Coulomb field of a target. The other is polarization bremsstrahlung (PB), which was first recognized in the 1970s [1,2]. It is a kind of radiation produced not by incident electrons but by the target atom's electrons as the atom is polarized. To be specific, the incoming electrons cause the polarization of the target atom by deforming the electronic density distribution of the target, and the emission of the photon in PB results from the dynamic changes of the polarization [3]. In addition to the distinction in the formation process, the features of PB that distinguish it from OB lie in the following aspects: first, PB has different dependencies on the mass and energy of the incident charged particle [4–7]; second, the angular distribution of PB is of a dipole nature and peaked at 90°, whereas OB has a more forward angular distribution [7].

The accurate description of EB helps in studying the physical mechanism of the collision of electrons and atoms. On the other hand, it plays an important role in materials science, astrophysics, radiology, and nuclear fusion [8]. For example, in fusion research, the precise calculation and measurement of EB spectra determine the accuracy of the β-ray-induced X-ray spectrometry (BIXS) technique for tritium analysis [9–13]; in the design of x-ray sources, the study of EB, which is one of the key processes for the collision between electrons and the target material, is also important.

In the 1970s, Tseng and Pratt presented a new standard for the calculation of OB [14], which was made available in a useful way with the tabulation of energy spectra [15] and finally the tabulation of the shape functions [16]. Then Seltzer and Berger published a table of bremsstrahlung cross sections for electrons with energies from 1 keV to 10 GeV and the atomic number range of 1–100 [17,18], which are the best theoretical results available at present and widely used in Monte Carlo simulations and comparisons with experimental data. Most recently, OB is still an interesting research topic [19–22]. However, the theory of PB needs to be further improved, although a lot of effort has been made. The emission of PB at relativistic energies was studied in 1985 [23,24], by treating the process within the framework of the relativistic plane-wave Born approximation for the projectile and in the nonrelativistic approximation for the target electrons [25]. The theoretical description of the photon spectrum that included a PB contribution was first provided with nonrelativistic approximation in the 1990s [4,26]. Then, a new method for the calculation of the bremsstrahlung spectrum including PB, which is called the stripping approximation (SA), was presented [27,28]. On account of its lacking the angular distribution and the interference between the OB and PB amplitudes, the SA theory is generally used to suggest the trend and estimate the contribution of PB [29].

One of the key researches on bremsstrahlung is seeking and confirming the contribution of PB to the EB spectra. In 2003, Sal Portillo and Quarles reported the measured absolute doubly differential cross sections for bremsstrahlung from Ne, Ar, Kr, and Xe rare-gas atoms at 28 and 50 keV incident electron energies and compared them with the theoretical models [29]. The significant discrepancies between the experimental data and theoretical results based only on OB provided definitive evidence for the existence of PB for gas targets [3,29–31]. In 2009, the absolute differential bremsstrahlung cross sections for 0.4–2-keV electrons scattered on Ar, Kr, and Xe atoms was also measured, and the experimental results are in obvious contradiction with the theory of OB [4]. In 2010, as shown in Ref. [5], the calculated results of PB cross sections fit well the experimental PB results produced by 0.7-keV electrons on

*Corresponding author: anzhu@scu.edu.cn
†Corresponding author: zhujingjun@scu.edu.cn

Xe atoms and clusters. Although the differences between the experimental data and the OB theory or OB theory plus PB stripping approximation [4,29] have not been quantitatively explained so far, these papers for gas targets [4,5,29] definitely showed that the PB exists when electrons impact gas targets.

However, there is still a hot debate about whether the PB contributes to the x-ray radiation spectra for solid targets. As stated in Ref. [32], no evidence for a PB contribution has been found because the measured absolute yields and doubly differential cross sections for bremsstrahlung radiated at 135° from 50-keV electrons on solid gold film were in good agreement with the PENELOPE predictions based only on OB. Absolute measurements of doubly differential electron-atom bremsstrahlung cross sections for several solid thin targets in the 20–100-keV energy region were also reported in 2018 and the agreement between the measured data and the OB theory was overall reasonable [33], as stated by the authors in their conclusions. Although some discrepancies observed between experiment and theory were inferred to be related to PB, they have not come to a definite conclusion, possibly because there were still errors in the experimental data that mainly derived from the determination of target thicknesses, the two-layer structure of targets, the effect of backscattered electrons, and the efficiency calibration of detectors, especially in the lower-energy region [33]. At present we cannot provide certain reasons for explaining the differences between the experimental data and the OB theory [33], and it needs further studies.

Unlike the thin-target bremsstrahlung mentioned above, the thick-target bremsstrahlung depends not only on the bremsstrahlung cross section but also on the electron energy loss and scattering in the target and the effect of secondary electrons produced in the target [34]. Nonetheless, the thick-target bremsstrahlung experiment avoids the large error caused by the determination of target thickness in the thin-target experiment. Some studies have reported measured bremsstrahlung spectra radiated at different angles for electron impact on a variety of thick solid targets and in general the agreement between experimental data for solid targets and Monte Carlo simulations based only on OB was good and concluded that there was no significant PB contribution to the total bremsstrahlung spectra for thick solid targets [8,35–38], although the differences between experiment and OB theory still existed. For example, a satisfactory agreement between the experimental spectra generated by 20- and 30-keV electron impact on some thick solid targets and the simulated spectra by using the Monte Carlo PENELOPE code [39], which is based only on OB, has been observed in the photon energy interval of 3–15 keV, but the differences in the low-energy region (<5 keV) between experiment and OB theory exist [35]. Besides, low-energy x-rays have been greatly absorbed by the 7- and 12.7-μm Be windows of the Si(Li) detectors used in Refs. [35,37] while possible PB contributions generally appeared in the low-energy x-ray region [40]. The results in Ref. [37] have also shown that the agreement is acceptable between the experimental spectra obtained from 5–25-keV electron impact on the thick targets and the simulated spectra by using the Monte Carlo PENELOPE code, but small discrepancies still exist in the lower- and higher-energy regions. The data processing method used in Ref. [37] did not consider the influence of the backscattered electrons escaped from the Faraday cup. In Ref. [38], a satisfactory agreement between the experimental and the Monte Carlo PENELOPE simulated spectra has also been found, and to prevent the escaped backscattered electrons from entering a C2 ultrathin window of a silicon drifted detector (SDD) x-ray detector (C2 window is a kind of "C-Series" x-ray ultrathin windows manufactured by Amptek, Inc.), a 7.05-μm aluminum film was placed in front of the SDD x-ray detector [38], which also resulted in absorptions of low-energy x-rays. As indicated in Ref. [41], discrepancies between the experimental spectra generated by 20-keV electron impact on thick targets and simulated results by using the PENELOPE code increase slightly with the atomic number of targets; i.e., for the medium-Z elements (Ti to Zr), the differences are about 6–7%, whereas for high-Z elements (Te to Au), the experimental spectra are about 10% higher than simulated spectra [41].

In particular, most recently, Singh *et al.* claimed that they have found a large PB contribution to the bremsstrahlung spectra for solid metallic targets by comparing the experimental spectra generated by the β-ray emitter with the theoretical results [40,42–45]. They presented that the contribution of PB decreases with increasing bremsstrahlung photon energies and increases with increasing atomic numbers of the metallic targets [46,47]. For example, for the Al target, the PB contribution to the total bremsstrahlung spectra generated by the β-ray emitter ^{90}Sr decreases from 27% at 1-keV to 1% at 14-keV photon energies; for the Pt target, it decreases from 30% at 1 keV to 1% at 26 keV [40]. In their experiments, as described in Ref. [42], they eliminated the contribution of internal bremsstrahlung, bremsstrahlung produced in the source material, and x-ray background in the experimental spectra by employing a Perspex β stopper technique and placing the target at positions A and B, which are before and after the β stopper. However, one point that should be noted is that the effect of the bremsstrahlung produced in the Perspex stopper on the experiment results has not been canceled [42]. Moreover, for the description of the thick-target bremsstrahlung, Monte Carlo simulation may be more suitable than the analytical method used in this paper [42] due to the complicated characteristics of the thick-target bremsstrahlung, for example, multiple scattering of electrons. Therefore, it still remains to further study whether there is PB contribution to the total spectra produced by electron impact on solid targets.

In this paper, we have measured the EB spectra produced by 5–25-keV electrons impacted on thick solid targets (Al ($Z = 13$), Cu ($Z = 29$), Ag ($Z = 47$), Te ($Z = 52$), and Au ($Z = 79$)) with high accuracy, and compared the experimental spectra with the simulated results by using the Monte Carlo code PENELOPE which has proved to be the most suitable for the calculation of electron-induced x-ray spectra, mainly because it incorporates realistic interaction cross sections and can be applied to describe any complex geometries [41]. Our main goal of this paper is to observe whether the OB theory can fit well the accurate experimental data for solid targets and identify whether the PB exists in the collisions of electrons with solid targets. Herein, Al, Ag, and Au are the "benchmark" elements in the theoretical calculations of Pratt

and Kissel, which have relatively higher calculation accuracy [15,16]. In comparison with previous experiments, some improvements have been made in this paper. For example, to ensure a high detection efficiency at the low-energy region of the x-ray spectra, we used an x-ray detector with a C2 ultrathin window instead of a thick Be window; moreover, the escaped backscattered electrons from the Faraday cup have been completely deflected by a permanent magnet pair, and we have also adopted new methods for data processing and performed detection efficiency calibration for the x-ray detector in low-energy regions (0.68–6 keV).

II. EXPERIMENT

A. Experimental setup

The experimental setup in this paper is similar to that in Refs. [48,49]. The whole setup was installed in the vacuum target chamber of a KYKY-2800B scanning electron microscope (SEM, KYKY Technology Co., Ltd., China) with a vacuum degree less than 3×10^{-3} Pa. Monoenergetic electron beams were emitted from the heated filament in the SEM. Accelerated by an electric field, the well-focused beams passed through the top hole of a copper Faraday cup vertically, then bombarded the thick targets. The wall thickness of the copper Faraday cup is 5 mm and could effectively prevent the high-energy bremsstrahlung photons from penetrating. For suppressing the escape of electrons with energies less than 100 eV, a bias voltage of -100 V was set in both the top hole and the side hole of the Faraday cup. We also calculated the escape rate of electrons with energies higher than 100 eV by Monte Carlo PENELOPE simulations. The electron-beam current was collected by an ORTEC digital current integrator, which has an accuracy of less than 1% for the charge measurement. X-rays that traversed through the side hole of the Faraday cup were measured by a horizontally placed SDD. With respect to the incident electrons, the target is tilted by 45°, and the angle of x-ray emission is 90°. The dead-time corrections for experimental x-ray spectra were negligible (<1%) because of the low electron-beam current intensities used in our experiments and the ability of SDD for high count rates.

The x-ray detector used in this experiment was the XR-100SDD manufactured by Amptek Inc., USA. There is a 25 mm^2 C2 ultrathin window in front of its sensitive volume, and its energy resolution for a 5.9-keV ^{55}Mn $K\alpha$ x-ray is 125 eV. The use of XR-100SDD with a C2 ultrathin window can decrease the absorption of low-energy x-rays and can detect the low-energy x-rays down to the boron $K\alpha$ line (0.183 keV).

The backscattered electrons that escaped from the side hole of the Faraday cup would lead to malfunction of the SDD. In view of this, a permanent magnet pair with 800 G designed with ANSYS MAXWELL software [50] (Westmag Technology Co., Ltd., China) was placed in front of the SDD for deflecting the backscattered electrons. We have simulated the trajectories of the backscattered electrons with different energies in the magnetic field by CST PARTICLE STUDIO [51], and confirmed that the permanent magnet pair is strong enough to deflect all backscattered electrons. The inspection report of the manufacturer shows that the magnetic field has hardly any leakage flux, so the effect of the magnet on other apparatus can be ignored.

The Al, Cu, Ag, Te, and Au thick targets used here were provided by Beijing Goodwill Metal Co., Ltd., China. The targets were 1.5 mm thick and the surfaces were polished. The diameters were 20 mm for the Au target and 31 mm for the other four targets. The purity of Ag was 99.95%, and it was 99.99% for the other four targets.

B. Detection efficiency calibration of SDD

The detection efficiency of a detector depends on the detector's sensitive volume, geometry, x-ray energy, and solid angle to the source (the distance from the source to the detector). The efficiency calibration of a detector not only plays an important role in the quantitative analysis of x-rays, but also can be used to verify the accuracy of the detector's geometrical parameters. There are several methods to determine the efficiency of the detector, among which the standard radioactive source method is the most widely used one. Therefore, in the high-energy region (>3.3 keV), the efficiency of the SDD was calibrated by the standard radioactive source method. The experimental conditions of the efficiency calibration were consistent with the conditions when the EB spectra were measured. Standard sources (^{55}Fe, ^{57}Co, ^{137}Cs, and ^{241}Am) with activity accuracies of 1–3% ($k = 2$) were supplied by the Physikalisch-Technische Bundesanstalt, Germany (PTB). The energies of the full-energy peaks were as follows:3.3, 11.89, 13.90, 17.81, 20.82, and 26.34 keV for ^{241}Am; 4.70, 32.10, 36.50, and 37.35 keV for ^{137}Cs; 6.40, 7.06, and 14.41 keV for ^{57}Co; and 5.90 and 6.49 keV for ^{55}Fe. As for ^{241}Am, the intensity emission of the 3.3-keV characteristic x-ray was taken from Ref. [52]. The half-lives, x-ray energies, and intensity emission rates of other standard sources were taken from the recommendation values of the International Atomic Energy Agency (IAEA) [53].

The standard radioactive source method is not feasible below 3.3 keV due to a lack of suitable radionuclide standards [54], although we are most concerned about the low-energy region. Hence, in this paper, the efficiency calibration of the SDD in the low-energy range has been accomplished by measuring characteristic x-ray spectra produced by 20-keV electron impact on various thick solid targets (i.e., characteristic peak method). The targets used here were also provided by Beijing Goodwill Metal Co., Ltd. and were as follows: MgF_2, Si_3N_4, WS_2, CaF_2, Ti, and Mn with purities higher than 99.9%. The ratios of the areas for characteristic peaks between experimental and simulated spectra before the C2 window of the SDD by the Monte Carlo PENELOPE code determined the shape of the detection efficiency curve in 0.68–6 keV. Finally, the absolute experimental efficiency values in the low-energy region were obtained by means of normalizing the shape of the efficiency values in the low-energy region to absolute efficiency values in the higher-energy region obtained with standard sources.

The detection efficiency of the SDD can be calculated by the following model [38]:

$$\varepsilon(E) = cT(E)T_{\mathrm{col}}(E)A(E), \tag{1}$$

where $T(E)$ presents the transmission coefficient of x-rays through the various absorption layers, $T_{\rm col}(E)$ is the transmittance of the collimator, and $A(E)$ is the absorption of x-rays in the detector sensitive volume; c is a normalized constant.

$$T(E) = \exp\left(-\mu_{Si_3N_4}x_{Si_3N_4} - \mu_{Al}x_{Al}\right), \quad (2)$$

$$T_{\rm col}(E) = \eta\left[1 + \frac{1-\eta}{\eta}\exp(-\mu_{\rm grid}x_{\rm grid})\right], \quad (3)$$

$$A(E) = 1 - \exp(-\tau_{Si}x_{\rm detector}), \quad (4)$$

where $\mu_{Si_3N_4}$, μ_{Al}, and $\mu_{\rm grid}$ describe the total mass attenuation coefficients of x-rays in the Si_3N_4 layer, Al layer, and Si grid for the C2 window, respectively; $x_{Si_3N_4}$, x_{Al}, $x_{\rm grid}$, and $x_{\rm detector}$ are the mass thickness values of the Si_3N_4 layer, Al layer, Si grid, and detector sensitive volume; τ_{Si} is the photoelectric absorption mass attenuation coefficient in the sensitive volume, and η presents the ratio of the opening area to the total area of the C2 window.

The total mass attenuation coefficients and the photoelectric absorption mass attenuation coefficients used in this paper are provided by the database of the PENELOPE code [39]. The geometry parameters of the SDD given by the manufacturer are as follows: 40-nm Si_3N_4 layer thickness, 30-nm Al layer thickness, 15-μm Si grid thickness, 78% open area ratio for C2 window, and 0.5-mm Si sensitive volume thickness. We can obtain the calculated efficiency curve by using Eq. (1) and the above parameters.

The errors of efficiency calibration by the standard source method mainly come from the activities of standard sources, the emission intensities of x-rays, the thickness of the polyethylene or polyester membrane covering on sources, and statistical counts. The errors are estimated to be 0.8–10% for various energy points of standard sources. For the characteristic peak method in the low-energy range, the errors are about 1%, mainly caused by the statistical errors of the experimental characteristic peaks and the statistical errors of the simulations by the PENELOPE code.

As shown in Fig. 1, the experimental efficiency values are in excellent agreement with the calculated efficiency curve based on the detector parameters provided by the manufacturer, which verifies the accuracy of the detector parameters provided by the manufacturer.

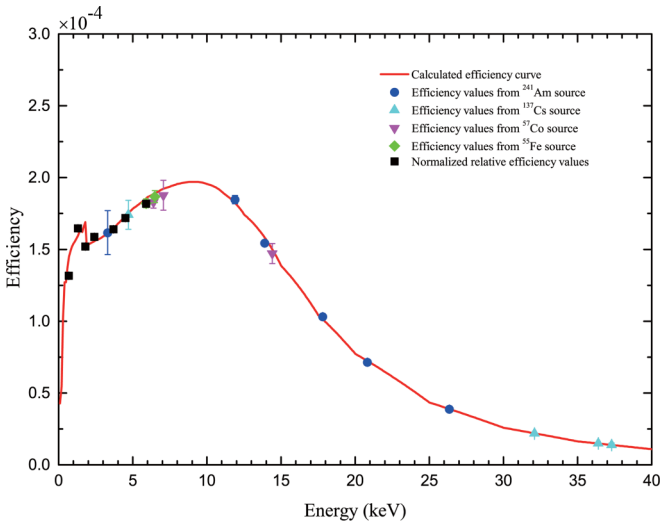

FIG. 1. The detection efficiency of the SDD. The calculated efficiency curve is based on Eq. (1) and the geometry parameters provided by the detector manufacturer. The total experimental efficiency values were obtained by normalizing the shape of efficiency values in the low-energy region to absolute efficiency values in the higher-energy region obtained with the standard sources.

III. MONTE CARLO SIMULATIONS

PENELOPE is a Monte Carlo simulation program developed by Salvat *et al.* [39], which implements a mixed simulation scheme combining the detailed simulation of hard events with a condensed simulation of soft events. It is available for simulating coupled electron-photon transport with an energy range of 50 eV to 1 GeV in arbitrary material consisting of homogeneous bodies. For the simulation of OB emission, the scaled cross-section tables from Seltzer and Berger [17,18] and the analytic angular distribution [8] based on the benchmark partial-wave shape functions of Kissel [16] are crucial theoretical foundations and used in the PENELOPE code. Moreover, the atomic inner-shell ionization cross sections by electron or positron impact based on the distorted-wave Born approximation (DWBA) [55,56] theory are used for simulations of characteristic x-ray emissions. Not only primary electrons, but also photons and the secondary radiation electrons produced by interactions in the target, can be tracked by PENELOPE [39].

The PENELOPE program consists mainly of material files, geometry files, and main programs and subroutines. Users can utilize the MATERIAL program to generate the material files and extract the necessary physical information of each material from the material database. The material database contains the interaction cross-section and atomic relaxation data of elements 1–92 and the composition data of 280 different materials. Based on geometry files, any material system formed from homogeneous bodies limited by quadric surfaces can be described. The results such as the energy and the angular distributions of particles that emerge from the material system, the average energy deposited in each body, etc., can be provided by the PENMAIN program that performs simulations of electron-photon transport in complex material structures [39]. To generate more specific information, users can define the impact detector or the energy-deposition detector [39]. In this paper, the main program PM-FIELD, which was included in the PENELOPE package, was used to simulate radiation transport in matter with static electromagnetic fields.

We used the energy-deposition detector in PENELOPE to record the energy-deposition information of particles in the detector sensitive volume during simulations where the geometry parameters corresponded to the experimental conditions. The polyethylene collimator in the side hole of the Faraday cup was also included in the PENELOPE simulations. To shorten the time of simulations, we set the half angle of the x-ray detector subtended to the center of the thick solid target to be 30°. It was found that the simulation results for 30° and 5° subtended half angles of the x-ray detector were identical [37]. It is worth nothing that the simulation results with PENELOPE for energies below 1 keV should be considered to qualitative

values or semiquantitative values [39]. The reasons for this are in the following two aspects: the accuracy of the interaction cross section is not good for the energies below 1 keV; on the other hand, the trajectory picture for electrons and positrons ceases to be applicable when the de Broglie wavelength is similar to or greater than the interatomic spacing [39]. Therefore, our only concern is the comparison between theory and experiment in the x-ray energies larger than 1 keV.

In addition, we have calculated the escape rates of electrons during the experiments by using the PENELOPE code. The escape rates were used to correct the total counts of incident electrons, N_0, in Eq. (5); otherwise, the escaped backscattered electrons and secondary electrons from the two holes of the Faraday cup would lead to underestimating the counts of incident electrons. For Al, Cu, Ag, Te, and Au targets, the escape rates are ∼2.2–2.3%, ∼2.8–3.1%, ∼3.0–3.5%, ∼3.0–3.6%, and ∼3.3–3.8% for different incident electron energies in this paper, respectively.

IV. RESULTS AND DISCUSSION

The response function of the SDD can be described very well by a linear combination of several analytical functions: a Gaussian profile for the x-ray principal component, and additional tail contributions (exponential tails and step functions) on the low-energy side of the x-ray line due to incomplete charge collections [57]. We convoluted the simulated spectra by the PENELOPE code with the above response functions instead of only a Gaussian distribution in Ref. [38]. The parameters of the exponential tail and step function for the SDD were taken from Ref. [57].

For the purpose of comparing the simulation spectra with the experimental spectra directly, all experimental spectra have been transformed into absolute intensity units by the following expression:

$$N(E) = \frac{N_x(E)}{N_0 \Delta\Omega \Delta E}, \tag{5}$$

where $N_x(E)$ is the number of x-ray counts in a particular photon energy channel by the detector, N_0 is the total number of incident electrons, $\Delta\Omega$ is the solid angle subtended by the detector, and ΔE is the energy channel width. In this work, $\Delta E = 30.93\,\text{eV/channel}$ and $\Delta\Omega = 2.84 \times 10^{-3}\,\text{sr}$ determined by the detector efficiency curve. The present data processing method is different from the previously used one [37,41] and can take into account the effects of secondary processes in the entrance window and the sensitive volume of the SDD.

The low-energy region of the x-ray spectrum is the most concerning region because the PB contributions most probably appear in the low-energy range [40]. The errors of these experimental data were mainly derived from the statistical count error (<2.8%), the error of the incident electron counts (∼1%) and the error of the solid angle subtended by the detector determined by efficiency calibration (∼1.4%). The estimated experimental total errors are less than 3.3% (<10 keV). The errors of the simulations by PENELOPE mainly come from statistical error, which is less than 3% (1σ, <10 keV).

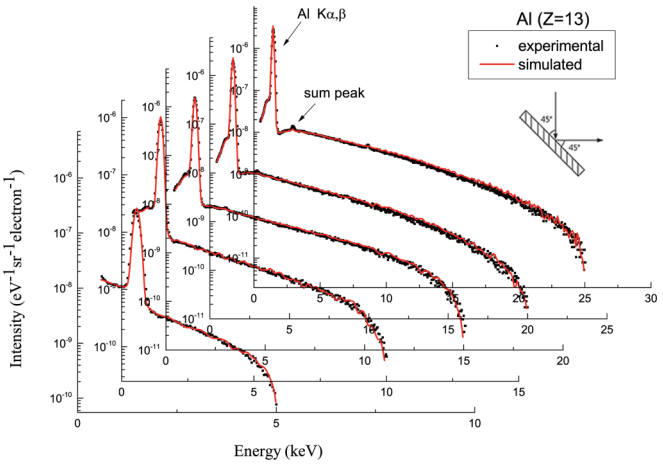

FIG. 2. The dots indicate the experimental spectra produced by 5–25-keV electron impact on thick Al targets, and the solid lines represent the simulated spectra obtained from the PENELOPE code.

Figures 2–6 are the comparisons between the experimental x-ray spectra produced by 5–25-keV incident electron impact on thick Al, Cu, Ag, Te, and Au targets and the simulated spectra by using the PENELOPE code. As explained in the previous section, the simulation results from the PENELOPE code are accurate and credible for the x-ray energies larger than 1 keV.

As shown in Fig. 2, the peak at 1.46 keV is the $K\alpha$ and $K\beta$ characteristic x-ray peak of Al. At about 3.0 keV, a sum peak of the Al peak appears in the experimental spectra produced by 20- and 25-keV incident electrons, which is due to the pulse pile-up effect. The measured bremsstrahlung spectra for the Al target are in excellent agreement with the simulated results by using the PENELOPE code.

In Fig. 3, the simulated spectra for the Cu target also have a good agreement with the experimental data except for the x-ray energies around 1.73 keV. The peak at 0.9 keV is the L-shell characteristic x-ray peak of Cu; the peaks at 8.0 and 8.9 keV are the $K\alpha$ and $K\beta$ characteristic peaks of the Cu target, respectively. The small peak at 1.73 keV in the experimental spectra probably comes from the interference of

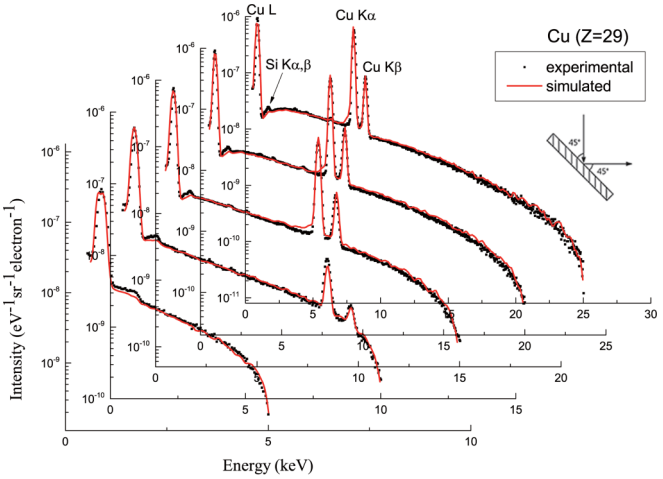

FIG. 3. The same as in Fig. 2, except for Cu.

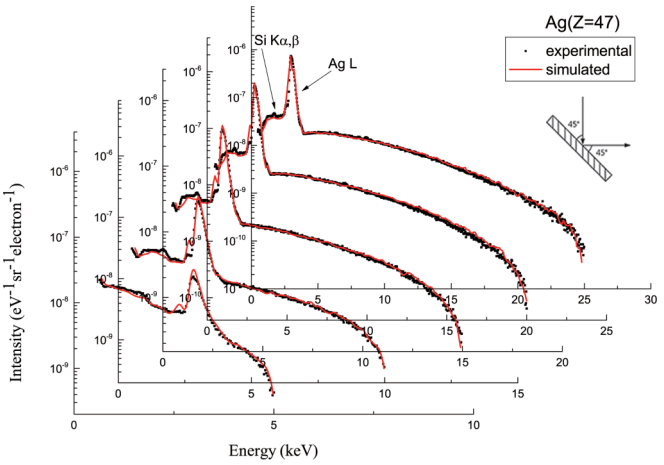

FIG. 4. The same as in Fig. 2, except for Ag.

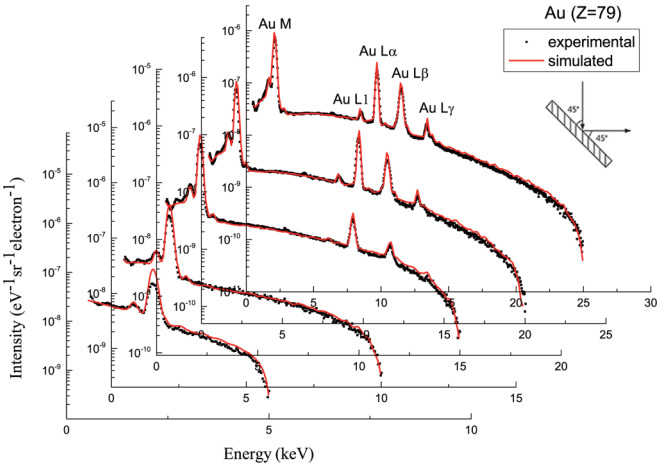

FIG. 6. The same as in Fig. 2, except for Au.

silicon material in the SDD as pointed out by the manufacturer [58]. Although the silicon material in the C2 window was included in the present PENELOPE simulations, the small peak at 1.73 keV was not well reproduced.

In Fig. 4, the peak at 2.97 keV is the L-shell characteristic x-ray peak of Ag. As mentioned above, the peak at 1.73 keV is probably related to the silicon material in the SDD. As for the small differences around 1 keV, we think that they are probably caused by other internal structural materials of the SDD which are not included in the PENELOPE simulations. As a whole, the agreement between the measured spectra and the simulated spectra is also very satisfactory for the Ag target for x-ray energies above 2 keV.

An excellent agreement between the experimental and the simulated spectra for the Te target is shown in Fig. 5. The peak at 3.8 keV is the L-shell characteristic peak of Te.

Figure 6 also shows a good agreement between the experimental and simulated results for the Au target. The peak at 2.12 keV is the M-shell characteristic x-ray peak of Au; the peaks at 9.7, 11.4, 13.4, and 8.5 keV are the $L\alpha$, $L\beta$, $L\gamma$, and $L1$ characteristic peaks of the Au target, respectively. Small differences at the characteristic x-ray peaks between the experimental and simulated results are probably caused by the inaccuracy of the inner-shell ionization cross sections or atomic relaxation parameters.

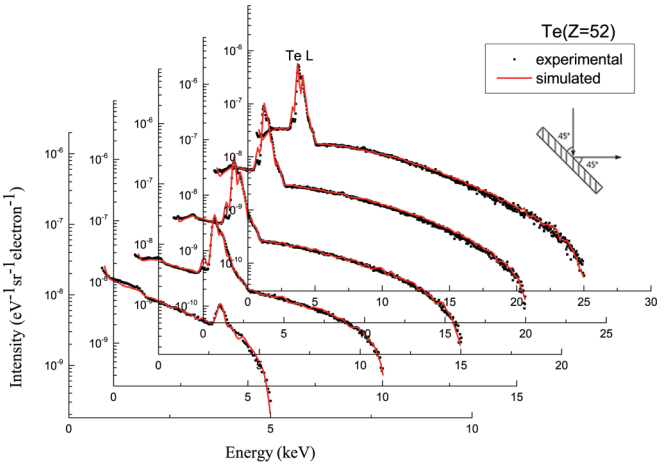

FIG. 5. The same as in Fig. 2, except for Te.

V. CONCLUSIONS

We have measured the bremsstrahlung spectra produced by 5–25-keV electrons bombarding on thick targets (Al ($Z = 13$), Cu ($Z = 29$), Ag ($Z = 47$), Te ($Z = 52$), and Au ($Z = 79$)) with high accuracy. The use of the SDD with a C2 ultrathin window and new methods for data processing and efficiency calibration ensured a high accuracy of the experimental data, especially in the lower-energy region; the interference of the backscattered electrons to the SDD has been completely eliminated by a permanent magnet pair. An excellent agreement has been found between the experimental spectra and the simulation results by using the Monte Carlo code PENELOPE which only contains the ordinary bremsstrahlung contribution. Our results show that there is no polarization bremsstrahlung contribution to the total bremsstrahlung spectra for electron impact on thick solid targets in the x-ray energy region larger than 1 keV. In comparison with the results of gas targets for which the polarization bremsstrahlung contribution has been definitely identified experimentally, a complete theory is needed urgently to explain the suppression of the polarization bremsstrahlung contributions in the x-ray radiation process for solid targets. The possible suppression mechanisms due to multiple scattering [30] and effects of the Coulomb field by neighboring atoms on the target atom [59] may be investigated in the future. In addition, it is also essential to consider the necessary conditions for the polarization bremsstrahlung's appearance, for example, the high polarizability of atoms and the particularities of atomic electron structure [4,60,61]. Moreover, the experimental results in this paper for thick solid targets do not question the experimental results for gas targets [4,29] and thin solid targets [33], in which some differences between the experiments and the theory cannot be explained at present and need further studies; our experimental data in this paper and in Ref. [62], together with the experimental data for gas targets [4,5,29] and thin solid targets [33], can be used as a database which can help further studies of bremsstrahlung of electron-atom collisions for gas targets and thin and thick solid targets.

[1] V. M. Buimistrov and L. I. Trakhtenberg, Zh. Eksp. Teor. Fiz. **69**, 108 (1975).

[2] M. Ya. Amusia, A. S. Baltenkov, and A. A. Paiziev, Sov. Phys. JETP Lett. **24**, 332 (1976).

[3] O. I. Obolensky and R. H. Pratt, Radiat. Phys. Chem. **75**, 2239 (2006).

[4] E. V. Gnatchenko, A. N. Nechay, and A. A. Tkachenko, Phys. Rev. A **80**, 022707 (2009).

[5] E. V. Gnatchenko, A. N. Nechay, V. N. Samovarov, and A. A. Tkachenko, Phys. Rev. A **82**, 012702 (2010).

[6] A. V. Korol and A. V. Solov'yov, J. Phys. B: At. Mol. Opt. Phys. **30**, 1105 (1997).

[7] V. Astapenko, *Polarization Bremsstrahlung on Atoms, Plasmas, Nanostructures and Solids* (Springer-Verlag, Berlin, 2013), Vol. 72, p. 4.

[8] E. Acosta, X. Llovet, and F. Salvat, Appl. Phys. Lett. **80**, 3228 (2002).

[9] M. Matsuyama, T. Tanabe, N. Noda, V. Philipps, K. H. Finken, and K. Watanabe, J. Nucl. Mater. **290–293**, 437 (2001).

[10] M. Matsuyama, N. Bekris, M. Glugla, N. Noda, V. Philipps, and K. Watanabe, J. Nucl. Mater. **313–316**, 491 (2003).

[11] Z. An, Q. Hou, and J. J. Long, Nucl. Instrum. Methods Phys. Res. B **266**, 3643 (2008).

[12] L. Mao, Z. An, J. H. Liang, X. G. Long, S. M. Peng, and W. G. Zhang, Nucl. Instrum. Methods Phys. Res. B **269**, 105 (2011).

[13] W. G. Zhang, H. W. Sun, F. Y. Zeng, L. Mao, Q. Q. Wu, J. J. Zhu, and Z. An, Nucl. Instrum. Methods Phys. Res. B **275**, 20 (2012).

[14] H. K. Tseng and R. H. Pratt, Phys. Rev. A **3**, 100 (1971).

[15] R. H. Pratt, H. K. Tseng, C. M. Lee, L. Kissel, C. MacCallum, and M. Riley, At. Data Nucl. Data Tables **20**, 175 (1977).

[16] L. Kissel, C. A. Quarles, and R. H. Pratt, At. Data Nucl. Data Tables **28**, 381 (1983).

[17] S. M. Seltzer and M. J. Berger, Nucl. Instrum. Methods Phys. Res. B **12**, 95 (1985).

[18] S. M. Seltzer and M. J. Berger, At. Data Nucl. Data Tables **35**, 345 (1986).

[19] A. Mangiarotti and M. N. Martins, Phys. Rev. A **94**, 022708 (2016).

[20] A. Poškus, Comput. Phys. Commun. **232**, 237 (2018).

[21] V. A. Yerokhin and A. Surzhykov, Phys. Rev. A **82**, 062702 (2010).

[22] D. H. Jakubassa-Amundsen, Phys. Rev. A **93**, 052716 (2016).

[23] M. Ya. Amus'ya, M. Yu. Kuchiev, A. V. Korol', and A. V. Solov'ev, Sov. Phys. JETP **61**, 224 (1985).

[24] V. A. Astapenko, V. M. Buimistrov, Yu. A. Krotov, L. K. Mikhailov, and L. I. Trakhtenberg, Sov. Phys. JETP **61**, 930 (1985).

[25] A. V. Korola and A. V. Solov'yov, Radiat. Phys. Chem. **75**, 1251 (2006).

[26] A. V. Korol, A. G. Lyalin, and A. V. Solov'yov, J. Phys. B: At. Mol. Opt. Phys. **30**, L115 (1997).

[27] N. B. Avdonina and R. H. Pratt, J. Phys. B: At. Mol. Opt. Phys. **32**, 4261 (1999).

[28] A. V. Korol, A. G. Lyalin, A. V. Solov'yov, N. B. Avdonina, and R. H. Pratt, J. Phys. B: At. Mol. Opt. Phys. **35**, 1197 (2002).

[29] S. Portillo and C. A. Quarles, Phys. Rev. Lett. **91**, 173201 (2003).

[30] C. A. Quarles and S. Portillo, Radiat. Phys. Chem. **75**, 1187 (2006).

[31] C. A. Quarles and S. Portillo, Nucl. Instrum. Methods Phys. Res. B **241**, 14 (2005).

[32] S. Williams and C. A. Quarles, Phys. Rev. A **78**, 062704 (2008).

[33] Juan A. García-Alvarez, José M. Fernández-Varea, Vito R. Vanin, and Nora L. Maidana, J. Phys. B: At. Mol. Opt. Phys. **51**, 225003 (2018).

[34] C. A. Quarles, Radiat. Phys. Chem. **59**, 159 (2000).

[35] E. Acosta, X. Llovet, E. Coleoni, J. A. Riveros, and F. Salvat, J. Appl. Phys. **83**, 6038 (1998).

[36] F. Salvat, J. M. Fernandez-Varea, J. Sempau, and X. Llovet, Radiat. Phys. Chem. **75**, 1201 (2006).

[37] L. X. Tian, J. J. Zhu, M. T. Liu, and Z. An, Nucl. Instrum. Methods Phys. Res. B **267**, 3495 (2009).

[38] W. J. Tan, Z. An, J. J. Zhu, J. L. Zhao, and M. T. Liu, Acta Phys. Sin. **65**, 113401 (2016).

[39] F. Salvat, J. M. Fernández-Varea, and J. Sempau, PENELOPE-2008: A Code System for Monte Carlo Simulation of Electron and Photon Transport, OECD/NEA Data Bank, Issy-les-Moulineau, France. 2009.

[40] A. Singh and A. S. Dhaliwal, Radiat. Phys. Chem. **119**, 167 (2016).

[41] X. Llovet, L. Sorbier, C. S. Campos, E. Acosta, and F. Salvat, J. Appl. Phys. **93**, 3844 (2003).

[42] T. Singh, K. S. Kahlon, and A. S. Dhaliwal, J. Phys. B: At. Mol. Opt. Phys. **41**, 235001 (2008).

[43] T. Singh, Nucl. Instrum. Methods Phys. Res. B **388**, 9 (2016).

[44] A. Singh, T. Singh, and A. S. Dhaliwal, Radiat. Phys. Chem. **141**, 207 (2017).

[45] S. J. Sharma, T. Singh, D. Singh, A. Singh, and A. S. Dhaliwal, Nucl. Instrum. Methods Phys. Res. B **401**, 33 (2017).

[46] A. Singh and A. S. Dhaliwal, Appl. Radiat. Isot. **115**, 190 (2016).

[47] A. Singh and A. S. Dhaliwal, Phys. Lett. A **379**, 1127 (2015).

[48] J. L. Zhao, Z. An, J. J. Zhu, W. J. Tan, and M. T. Liu, J. Phys. B: At. Mol. Opt. Phys. **49**, 065205 (2016).

[49] J. L. Zhao, Z. An, J. J. Zhu, W. J. Tan, and M. T. Liu, Radiat. Phys. Chem. **134**, 71 (2017).

[50] https://www.ansys.com/products/electronics/ansys-maxwell

[51] H. Spachmann and U. Becker, Nucl. Instrum. Methods Phys. Res. A **558**, 50 (2006).

[52] W. J. Gallagher and S. J. Cipolla, Nucl. Instrum. Methods **122**, 405 (1974).

[53] M.-M. Bé, V. Chisté, C. Dulieu *et al.*, International Atomic Energy Agency, Vienna, December 2005, http://www-nds.iaea.org/xgamma_standards/

[54] I. Uzonyi, Gy. Szabo, I. Borbely-Kiss, and A. Z. Kiss. Nucl. Instrum. Methods Phys. Res. B **210**, 147 (2003).

[55] S. Segui, M. Dingfelder, and F. Salvat, Phys. Rev. A **67**, 062710 (2003).
[56] D. Bote and F. Salvat, Phys. Rev. A **77**, 042701 (2008).
[57] G. Calzolai, S. Tapinassi, M. Chiari, M. Giannoni, S. Nava, G. Pazzi, and F. Lucarelli. Nucl. Instrum. Methods Phys. Res. B **417**, 51 (2018).
[58] http://amptek.com/products/c-series-low-energy-x-ray-windows/#8
[59] S. Requena, S. Williams, and C. A. Quarles, Nucl. Instrum. Methods Phys. Res. B **268**, 3561 (2010).
[60] B. A. Zon, Sov. Phys. JETP **46**, 65 (1977).
[61] Y. Morimoto, R. Kanya, and K. Yamanouchi, Phys. Rev. Lett. **115**, 123201 (2015).
[62] L. Li, Z. An, J. J. Zhu, and M. T. Liu, Nucl. Instrum. Methods Phys. Res. B **445**, 13 (2019).